LBL-9491 c. 2
Preprint

Lawrence Berkeley Laboratory
UNIVERSITY OF CALIFORNIA

Materials & Molecular Research Division

Submitted to the Journal of Chemical Physics

DECAY DYNAMICS OF THE CN*($B^2\Sigma^+$) AND XeF* ($B^2\Sigma^+$ AND $C^2\Pi_{3/2}$) STATES

E. D. Poliakoff, S. H. Southworth, M. G. White, G. Thornton,
R. A. Rosenberg, and D. A. Shirley

RECEIVED
LAWRENCE
BERKELEY LABORATORY

OCT 15 1979

LIBRARY AND
DOCUMENTS SECTION

July 1979

TWO-WEEK LOAN COPY

This is a Library Circulating Copy
which may be borrowed for two weeks.
For a personal retention copy, call
Tech. Info. Division, Ext. 6782

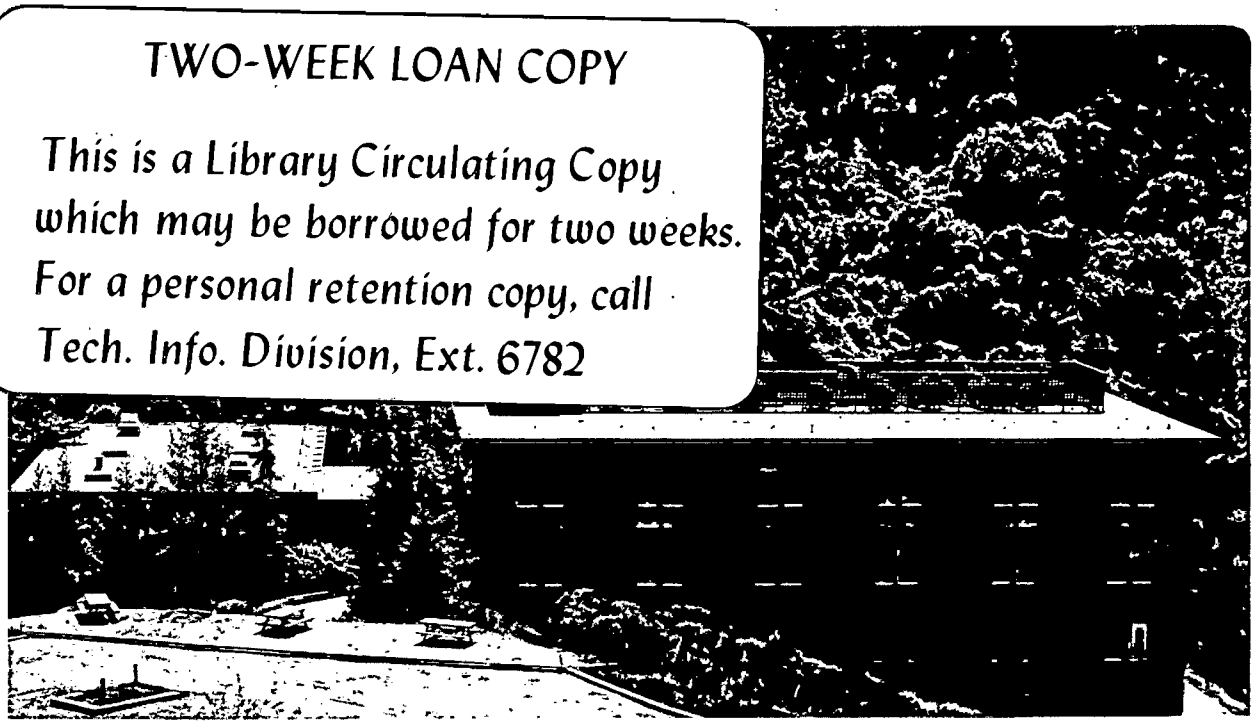

LBL-9491 c.2

Prepared for the U.S. Department of Energy under Contract W-7405-ENG-48

DISCLAIMER

This document was prepared as an account of work sponsored by the United States Government. While this document is believed to contain correct information, neither the United States Government nor any agency thereof, nor the Regents of the University of California, nor any of their employees, makes any warranty, express or implied, or assumes any legal responsibility for the accuracy, completeness, or usefulness of any information, apparatus, product, or process disclosed, or represents that its use would not infringe privately owned rights. Reference herein to any specific commercial product, process, or service by its trade name, trademark, manufacturer, or otherwise, does not necessarily constitute or imply its endorsement, recommendation, or favoring by the United States Government or any agency thereof, or the Regents of the University of California. The views and opinions of authors expressed herein do not necessarily state or reflect those of the United States Government or any agency thereof or the Regents of the University of California.

DECAY DYNAMICS OF THE $CN^*(B^2\Sigma^+)$ AND $XeF^*(B^2\Sigma^+$ AND $C^2\Pi_{3/2})$ STATES

E.D. Poliakoff, S.H. Southworth, M.G. White, G. Thornton,
R.A. Rosenberg, and D.A. Shirley

Materials and Molecular Research Division
Lawrence Berkeley Laboratory
and
Department of Chemistry
University of California
Berkeley, California 94720

July 1979

ABSTRACT

The fluorescence decay of $CN^*(B^2\Sigma^+)$ and $XeF^*(B^2\Sigma^+$ and $C^2\Pi_{3/2})$ radicals has been investigated following photodissociation of ICN and XeF_2, respectively. Pulsed synchrotron radiation from the Stanford Synchrotron Radiation Laboratory was used as an excitation source so that the fluorescence decay could be monitored directly. Pressure-dependent studies were carried out to separate the effects of collisional quenching from those of radiative decay. The radiative lifetimes derived for the $CN^*(B^2\Sigma^+)$, $XeF^*(B^2\Sigma^+)$, and $XeF^*(C^2\Pi_{3/2})$ radicals are 70.5 ± 2 nsec, 14.2 ± 0.2 nsec, and 98 ± 10 nsec, respectively. The collisional fluorescence quenching rate for the $CN^*(B^2\Sigma^+)$ state by ICN was determined to be $(1.15 \pm 0.04) \times 10^{-9} cm^3 \cdot s^{-1}$ (294 K). In addition to the $CN^*(B^2\Sigma^+)$ fluorescence observed from ICN excitation, a very fast fluorescence component was observed which is attributed to radiative decay of valence (and/or Rydberg) excitations in ICN.

I. Introduction

The radiative lifetimes of $CN^*(B^2\Sigma^+)$ and $XeF^*(B^2\Sigma^+$ and $C^2\Pi_{3/2})$ have been the subjects of intense study. The $CN(B \rightarrow X)$ transitions are observed in many astrophysical systems,[1a,b] and calculations of the CN radical concentrations are dependent on accurate values for the strength of this transition. In addition, there have been many determinations of the $CN^*(B^2\Sigma^+)$ lifetime leading to different values. Lifetime measurements on the $XeF^*(B^2\Sigma^+)$ state are motivated by two reasons. First, the $XeF(B \rightarrow X)$ transitions contain several lasing lines, and the lasing gain depends on the lifetime of the upper level. Second, the electronic structure of XeF has been a topic of current interest because of its relatively large ground-state dissociation energy.[2,3] The radiative lifetimes of excited states of XeF serve as stringent tests of theoretical wavefunctions used to compute the electronic structure of this radical.

Synchrotron radiation has the capacity to be a useful tool for the study of radiative decay following photodissociation. In particular, the pulse structure at Stanford Synchrotron Radiation Laboratory (SSRL) allows one to follow the radiative decay on a nanosecond time scale. Recent studies on atomic,[4a-c] molecular,[5,6,7] and solid-state[8] systems have exploited the timing characteristics of synchrotron radiation[9] to study dynamic processes of excited states. One can also photodissociate a molecule using a synchrotron radiation pulse, producing electronically excited fragments, and study the radiative decay of the fragments. This is the nature of the work reported here, where excited-state radicals, CN* and XeF*, have been produced via photodissociation of ICN and XeF_2, respectively.

Section II contains a description of the experiment; Section III discusses the data reduction and states the results. Straightforward kinetic modeling of the data is presented in Section IV. Section V contains conclusions.

II. Experimental

The experimental setup has been described in a previous publication,[4a] so only a brief description is given here. A schematic diagram of the experimental arrangement is shown in Fig. 1. Radiation at SSRL is pulsed with a 0.4 nsec pulse width and a 780 nsec repetition period. On the 8° branch line of Beam Line I, where this work was performed, photons with 4 eV $\leqslant h\nu \leqslant$ 34 eV are available. A LiF window separated our chamber from the ultrahigh vacuum of the beam-line optics, limiting our usable photon energy range to 4 eV $\leqslant h\nu \leqslant$ 11.8 eV. The wavelength bandwidth of the excitation radiation was 2.5 A, providing a nominal photon flux of 10^{10} photons/sec.

Pressure measurement was done using a capacitance manometer (MKS #315 BHS-10) while the samples were in a flow system. In the case of the XeF_2 sample, the pressure measurement was not absolute because a conductance-limiting valve was placed between the capacitance manometer and the interaction volume. Thus, collisional quenching rates could not be determined absolutely although the intercepts from the extrapolation yielded reliable zero-pressure radiative lifetimes.

The ICN sample ($\geqslant$99.5% pure) was obtained from Eastman Kodak and was used without further purification. ICN sample pressure was varied between 4.7×10^{-3} Torr and 0.486 Torr.

The XeF_2 sample was ≥99.9% pure for the volatile components. Our measurements used XeF_2 pressures between 0.0175×10^{-2} and 1.21 Torr. The fluorescence detection photomultiplier tube (RCA C31000 M) was placed perpendicular to both the propagation vector and the $\underset{\sim}{\varepsilon}$ vector of the exciting radiation.

A fluorescence excitation spectrum of ICN was recorded at a sample pressure of 8×10^{-3} Torr. The fluorescence photons were time-gated such that only photons arriving within 60 nsec of the excitation pulse were counted. This was done to ensure that the excitation spectrum would not contain significant contributions from the $A^2\Pi$ system, which is much longer-lived ($\tau_{CN^*(A^2\Pi)} \geqslant 6$ μsec)[11] than the $B^2\Sigma^+$ state of CN*.

Fluorescence decay curves were taken at the following excitation wavelengths: 1698 Å, 1575 Å, 1480 Å, and 1402 Å. A discussion of the timing electronics is contained in Ref. 4. The present measurements employed an interference filter (Microcoatings, Inc., #3850 BBC, peak transmission at 3850 Å, FWHM = 200 Å) to pass only the CN(B → X) emissions.[16] At each wavelength, decay curves were obtained at four sample pressures to extrapolate out collisional effects. For XeF_2, the excitation wavelength was set at 1690 Å, exceeding thresholds for $XeF^*(B^2\Sigma^+)$ and $XeF^*(C^2\Pi_{3/2})$ production. All experiments were carried out at ambient temperature, ∿294° K.

III. Results

A. ICN

The fluorescence excitation spectrum is shown in Fig. 2. Spectral assignments are discussed in Refs. 12-14, but are not of direct interest

here, since the present study is concerned with fragment fluorescence. There is a strong similarity between fragment fluorescence yield and absorption spectra. The arrows in Fig. 2 denote wavelengths where decay curves were recorded. All the CN* decay curves discussed to this point were obtained with an interference filter (passing only $CN(B \rightarrow X)$ fluorescence) in front of the fluorescence detector.

It was found that all decay curves from experiments that used the interference filter could be fitted well by the form

$$I(t) = C_o + C_1[\exp - t/\tau]. \qquad (1)$$

A typical $CN^*(B^2\Sigma^+)$ decay curve is shown in Fig. 3. At each wavelength a plot of τ^{-1} vs pressure yielded a straight line; i.e., Stern-Volmer quenching behavior was observed.[15] A linear least-squares fit of τ^{-1} vs pressure was done at each excitation wavelength, and the results are shown in Fig. 4 and summarized in Table 1. In addition, a linear least-squares fit of τ^{-1} vs pressure was done using data points from all four excitation wavelengths. This fit is shown in Fig. 5 and the results are also given in Table 1. When the filter was not in place, two-component decays were observed consisting of the $CN^*(B^2\Sigma^+)$ decay component and a very fast component with $\tau < 2$ nsec (see Fig. 6). The lifetimes of this short component were not accurately determined because our instrumental response function was too long (approximately gaussian in time with $\sim$4 nsec FWHM). However, for each decay curve the integrated intensity of the short component was obtained by fitting the long ($CN^*(B^2\Sigma^+)$) component, subtracting out its contribution (as well as the constant background), and summing the photon counts remaining (which

are attributed to the fast decay). The integrated intensity of the long component is given by

$$I^{tot}_{CN(B^2\Sigma^+)} = \int_0^\infty c_1 e^{-t/\tau} dt = c_1\tau \qquad (2)$$

The results of these calculations are given in Table 2. The validity of these results are discussed in Section IV.

B. XeF_2

The XeF* decay curves were fitted to an equation of the form

$$I(t) = C_o + C_1 \exp(-t/\tau_1) + C_2 \exp(-t/\tau_2) \qquad (3)$$

A typical decay curve with its least-squares fit is shown in Fig. 7. Plots of both τ_1^{-1} and τ_2^{-1} vs pressure yielded straight lines (See Fig. 8). Each set of data was fitted with linear least-squares and the results are τ_1 = 14.2 ± 0.2 nsec and τ_2 = 98 ± 10 nsec. These fits yield decay parameters with larger relative uncertainties than the CN*($B^2\Sigma^+$) data which is attributed to the correlation between a large background parameter and the exponential decay parameters.

IV. Discussion

A. ICN

The kinetic analysis of the ICN data is quite straightforward. The photodissociation can be viewed as instantaneous;[16] thus, the 0.4 nsec excitation pulse defines the time zero of CN*($B^2\Sigma^+$) production.

At this juncture, we note that the predissociation event is not being analyzed and will not be discussed at length; but the predissociation event is significant in that it is much faster than the fluorescence process of $CN^*(B^2\Sigma^+)$. Quantitatively, we note that the convolution integral

$$I^{obs}(t) = \int_0^t \exp[-(t-t')/\tau_{CN^*(B^2\Sigma^+)}]f(t')dt \tag{4}$$

gives the intensity of $CN^*(B^2\Sigma^+)$ fluorescence as a function of time. Here $f(t')$ is the convoluting function, which describes the production of $CN^*(B^2\Sigma^+)$ as a function of time. If we equate $f(t') = \delta(t_o - t')$, then Eq. (4) reduces to the form $I(t) \propto \exp[-t/\tau_{CN^*(B^2\Sigma^+)}]$.

The results of Section III-A can thus be rationalized using the following kinetic scheme

$$h\nu + ICN \xrightarrow{\text{instantaneous}} I(^2P_{1/2,3/2}) + CN^*(B^2\Sigma^+)$$

$$\xrightarrow{\text{instantaneous}} I(^2P_{1/2,3/2}) + CN^*(A^2\Pi) \tag{5a}$$

$$\xrightarrow{\text{instantaneous}} I(^2P_{1/2,3/2}) + CN\ (X^2\Sigma^+)$$

$$CN^*(B^2\Sigma^+) \xrightarrow{\tau^{-1}_{CN^*(B^2\Sigma^+)}} CN(X^2\Sigma^+) + h\nu \tag{5b}$$

$$ICN + CN^*(B^2\Sigma^+) \xrightarrow{k_q^{ICN}} CN(X^2\Sigma^+,\ A^2\Pi) + ICN \tag{5c}$$

which yields the fluorescence intensity given by

$$I(t) = I^{o} \exp[-t/\tau(P)] \tag{6a}$$

where

$$[\tau(P)]^{-1} = \tau^{-1}_{CN^*(B^2\Sigma^+)} + k_q^{ICN} \cdot P \tag{6b}$$

Production of $CN^*(B^2\Sigma^+)$ by collisional conversion of $CN^*(A^2\Pi)$ has been neglected in this analysis for reasons noted by Duric et al.[11] Thus, the intercepts derived in Section III-A (see Table 1) are estimates of $\tau_{CN^*(B^2\Sigma^+)}$ and the slopes are quenching constants, k_q^{ICN}. The lifetime values vary with excitation wavelength. It is likely that this is caused by population of different rotational and vibrational distributions in the $CN^*(B^2\Sigma^+)$ manifold.

Radford and Broida have shown[17] that selected rovibronic levels in the $CN^*(B^2\Sigma^+)$ are strongly mixed with rovibronic levels of the $A^2\Pi$ system due to "L-uncoupling" terms in the molecular Hamiltonian. Jackson[18] measured lifetimes of the individual rotational levels in the $CN^*(B^2\Sigma^+, v' = 0)$ manifold and found that the perturbed rotational levels have lifetimes longer than the unperturbed rotational levels. However, many rotational levels are populated by the photodissociation.[23] Since the measured lifetime is a weighted average over the manifold of populated rotational levels and the density of perturbed rotational levels is small, it is unlikely that the variations in our measured lifetimes are due to perturbations of isolated rotational levels.

A more likely explanation is that the vibrational distribution changes with the excitation wavelength. This results in a change in the lifetime because of variations of lifetime with vibrational level (see Ref. 11, for example). Therefore, the present results suggest that

an investigation of vibrational distributions obtained with well-defined excitation wavelength be performed (as opposed to the work of Mele and Okabe,[23] where more than one discrete line was present in their resonance lamp excitation source).

Since our data do not give lifetimes of individual vibronic levels, we simply report the nominal lifetime of the $CN^*(B^2\Sigma^+)$ state as 70.5 ± 1.6 nsec (Table 1), and a quenching constant of $1.15(4) \times 10^{-9} cm^3 \cdot s^{-1}$, which is in good agreement with the work of Jackson and Faris.[24] The lifetime result that we report is larger than most of the results listed in Table 3. A possible reason for this discrepancy is that our work did not use a monochromator to analyze the fluorescence wavelength. The CN* fragments have a great deal of translational energy following photodissociation[23,24] and the same is presumably true of electron-impact dissociation. As shown by Mele and Okabe,[23] the CN fragment has approximately 1 eV in translational energy, and will move distances on the order of millimeters during its radiative lifetime. Depending on the position of the monochromator entrance slits and focusing optics leading to them, an excited CN* fragment might be out of the field of view of the monochromator if it fluoresces many nanoseconds after excitation. Thus, an apparent shortening of the lifetime will be observed due to the high degree of translational energy imparted to the $CN^*(B^2\Sigma^+)$ fragment.

This reasoning draws support from other investigators. The work of Luk and Bersohn[16] used both ICN and BrCN as $CN^*(B^2\Sigma^+)$ sources. One expects that the CN* fragment obtains more momentum (velocity) when it is fragmented from the heavier partner, i.e., the I atom. If the reasoning of the previous paragraph is correct, then the lifetime

determined by Luk and Bersohn from the ICN sample should be shorter than that obtained from their BrCN sample. In fact, they observed that $\tau_{CN^*(B^2\Sigma^+)} = 59.9 \pm 2.1$ nsec when ICN was used, and $\tau_{CN^*(B^2\Sigma^+)} = 61.7 \pm 0.1$ nsec when BrCN was the $CN^*(B^2\Sigma^+)$ source. Although the use of an interference filter in the fluorescence channel might yield less detailed information about specific rovibronic lifetimes, it will not introduce the artifact of a short lifetime since the excitation region and the fluorescing region are both in the field of view of the detector. For completeness, we note that the work of Jackson[18] was performed with thermalized CN fragments; thus, these arguments in no way affect his conclusions.

Some of our work did not use interference filters as discussed in Section III-A. A two-component decay was then observed. The additional component is attributed to fluorescence of ICN* molecules that do not predissociate. Because our phototube could not detect the resonance fluorescence of ICN, but only fluorescence to high vibrational levels of the ICN ground electronic state manifold, the ratios listed in Table 2 are lower limits to the true branching ratio of fluorescence to predissociation. No efforts at calibrated actinometry were performed, but the present results provide impetus for further work.

B. XeF_2

Decay of $XeF^*(B^2\Sigma^+$ and $C^2\Pi_{3/2})$ can be modeled simply using the following scheme:

$$XeF_2 + h\nu \xrightarrow{k_1} XeF^*(B^2\Sigma^+) + F$$
$$XeF_2 + h\nu \xrightarrow{k_2} XeF^*(C^2\Pi_{3/2}) + F$$

(instantaneous) (7a)

$$XeF^*(B^2\Sigma^+) + XeF_2 \xrightarrow{k_3} XeF^*(C^2\Pi_{3/2}) + XeF_2 \quad (7b)$$

$$XeF^*(C^2\Pi_{3/2}) + XeF_2 \xrightarrow{k_4} XeF^*(B^2\Sigma^+) + XeF_2 \quad (7c)$$

$$XeF^*(B^2\Sigma^+) + XeF_2 \xrightarrow{k_5} XeF(X^2\Sigma^+) + XeF_2 \quad (7d)$$

$$XeF^*(C^2\Pi_{3/2}) + XeF_2 \xrightarrow{k_6} XeF(X^2\Sigma^+) + XeF_2 \quad (7e)$$

$$XeF^*(B^2\Sigma^+) \xrightarrow{k_7 (=\tau^{-1}_{B^2\Sigma^+})} XeF(X^2\Sigma^+) + h\nu' \quad (7f)$$

$$XeF^*(C^2\Pi_{3/2}) \xrightarrow{k_8 (=\tau^{-1}_{C^2\Pi_{3/2}})} XeF(A^2\Pi) + h\nu'' \quad (7g),$$

where eqs. (7a) refer to excitation, (7b) and (7c) to collisional conversion, (7d) and (7e) to collisional quenching, (7f) and (7g) to radiative decay. As in ICN, the formation of the excited state radicals is assumed to be instantaneous. Omitting the excitation step, this kinetic model yields the following coupled differential equations:

$$\frac{-dC_B}{dt} = [k_7 + (k_3 + k_5)C_{XeF_2}]C_B - k_4\, C_{XeF_2} C_C \quad (8a)$$

$$\frac{-dC_C}{dt} = [k_8 + (k_4 + k_6)C_{XeF_2}]\, C_C - k_3\, C_{XeF_2}\, C_B \quad (8b)$$

where C_i denotes the concentration of the ith species (for brevity, B and C denote the $XeF^*(B^2\Sigma^+_{1/2})$ and $XeF^*(C^2\Pi_{3/2})$, respectively). The solutions to these equations are[25]

$$C_i = k_i^+ e^{m_+ t} + k_i^- e^{m_- t} \tag{9}$$

where i denotes $XeF^*(B^2\Sigma^+)$, $XeF^*(C^2\Pi_{3/2})$ and

$$m_\pm = \frac{-(a+c) \pm [(a-c)^2 + 4bd]^{1/2}}{2} \tag{10}$$

and where

$$a = k_7 + (k_3 + k_5) C_{XeF_2} \tag{11a}$$

$$b = k_4 C_{XeF_2} \tag{11b}$$

$$c = k_8 + (k_4 + k_6) C_{XeF_2} \tag{11c}$$

$$d = k_3 C_{XeF_2} \tag{11d}$$

which can easily be equated with coefficients of the concentration variables in eqs. (8a) and (8b). One can see from eq. (10) that $m_+ = -c$ and $m_- = -a$ when $4bd \ll (a-c)^2$. This condition is met, and can be verified by using our values of a and c (to be derived shortly) and using nominal values of transfer rates, b and d, from the literature.[26] Thus, eq. (9) can be written as

$$\begin{aligned} C_i = {} & k_i^+ \exp\{-[k_8 + (k_4+k_6)\ C_{XeF_2}]t\} \\ & + k_i^- \exp\{-[k_7 + (k_3+k_5)\ C_{XeF_2}]t\} \end{aligned} \tag{12}$$

The light intensity, I(t), can be written

$$I(t) = E_B \frac{dC_B}{dt} + E_C \frac{dC_C}{dt} \tag{13}$$

where the E_i's represent the efficiency of the photomultiplier tube detector to radiations from the B and C states. Since our phototube had an uncalibrated spectral response, we shall simply write

$$\begin{aligned} I(t) &= k_1 \exp\{-[k_8 + (k_4 + k_6)C_{XeF_2}]t\} \\ &+ k_2 \exp\{-[k_7 + (k_3 + k_5)C_{XeF_2}]t\} \end{aligned} \tag{14}$$

where k_1 and k_2 are taken as unknowns. This in no way detracts from the information contained in the arguments of the exponentials as functions of pressure. Eq. (14) implies that a two-exponential decay will be observed and that both decay components will vary linearly with pressure, as was observed. Thus, we conclude that τ_1 and τ_2 (see Section III-B) are equated with $[k_7 + (k_3 + k_5)C_{XeF_2}]$ and $[k_8 + (k_4 + k_6)C_{XeF_2}]$, respectively. Therefore, $\tau_{B^2\Sigma^+} = 14.2 \pm 0.2$ nsec and $\tau_{C^2\Pi_{3/2}} = 98 \pm 10$ nsec, which are in good agreement with previous investigations, as seen in Table 4. As was previously noted, the pressure was uncalibrated for the XeF_2 measurements, so the absolute values of the slopes of τ_i^{-1} vs pressure plots are unreliable. The radiative lifetimes obtained are reliable, because they are derived from the intercepts, not the slopes of the extrapolations.

V. Conclusions

The lifetime and ICN quenching constant of $CN^*(B^2\Sigma^+)$ have been determined to be 70.5 ± 1.6 nsec and $1.15 \pm 0.04 \times 10^{-9} cm^3 \cdot sec^{-1}$, respectively. This lifetime is in fair agreement with earlier investigations, although some discrepancy remains. It is possible that the high translational temperature of CN following dissociation led to artifacts in the previous investigations.

The lifetimes of the XeF^* $B^2\Sigma^+$ and $C^2\Pi_{3/2}$ states have been measured as 14.2 ± 0.2 nsec and 98 ± 10 nsec, in good agreement with calculations of Dunning and Hay[2] and with some previous investigations.

This work shows the value of synchrotron radiation as a tool for generating and probing excited-state radicals. However, the non-specificity of the photodissociation event implies that many rovibronic levels of the fragment will be populated. For detailed studies (e.g., monochromatized fluorescence for state distributions), intensity considerations preclude the use of synchrotron radiation for many systems. Finally, the timing characteristics of some synchrotron radiation facilities are superior to any existing VUV lasers and will also allow the study of electronic relaxation processes occurring on a nanosecond time scale.

ACKNOWLEDGMENTS

We thank Mr. Francis Tanzella and Professor Neil Bartlett for providing us with the XeF_2 sample.

This work was supported by the Division of Chemical Sciences, Office of Basic Energy Sciences, U.S. Department of Energy under Contract No. W-7405-Eng-48. It was performed at the Stanford Synchrotron Radiation Laboratory, which is supported by the NSF Grant No. DMR 77-27489, in cooperation with the Stanford Linear Accelerator Center.

REFERENCES

1. a) J.A. Myer and R.W. Nicholls, Nature 225, 928 (1970) and references therein.

b) R.J. Spindler, J. Quant. Spectrosc. Radiat. Transfer. 5, 165 (1965) and references contained therein.

2. T.H. Dunning and P.J. Hay, J. Chem. Phys. 69, 134 (1978).

3. C.H. Becker, P. Casavecchia, and Y.T. Lee, J. Chem. Phys. 69, 2377 (1978).

4. a) E. Matthias, R.A. Rosenberg, E.D. Poliakoff, M.G. White, S.-T. Lee, and D.A. Shirley, Chem. Phys. Lett. 52, 239 (1977).

b) E. Matthias, M.G. White, E.D. Poliakoff, R.A. Rosenberg, S.-T. Lee, and D.A. Shirley, Chem. Phys. Lett. 54, 30 (1978).

c) R.A. Rosenberg, M.G. White, E.D. Poliakoff, G. Thornton, and D.A. Shirley, J. Phys. B11, L719 (1978).

5. G. Thornton, E.D. Poliakoff, E. Matthias, S.H. Southworth, R.A. Rosenberg, M.G. White, D.A. Shirley, J. Chem. Phys. 71, 133 (1979).

6. H.D. Wenck, S.S. Hasnain, M.M. Nitikin, K. Sommer, G. Zimmerer, and D. Haaks, DESY report SR-79/07 (1979).

7. T.D. Bonfield, F.H.K. Rambow, G.K. Walters, M.V. McCusker, D.C. Lorents, and R.A. Gutchek, SSRL Report 78/09 (1978).

8. K.M. Monahan and V. Rehn, J. Chem. Phys. 68, 3814 (1978).

9. The time structure of a synchrotron is dependent on the length of the orbit as well as the number of electron bunches circulating through the accelerating ring. Several facilities have physical parameters well-suited for studying events on a nanosecond time

scale. A review of synchrotron radiation properties is given in: I. Lindau and H. Winick, Comments Atomic Mol. Phys. 6, 133(1977).

10. G.A. West and M.J. Berry, Chem. Phys. Lett. 56, 423 (1978).

11. N. Duric, P. Erman, and M. Larsson, Physica Scripta 18, 39 (1978).

12. G.W. King and A.W. Richardson, J. Mol. Spec. 21, 339 (1966).

13. M.T. Macpherson and J.P. Simons, J. Chem. Soc., Faraday II, in press.

14. J.W. Rabalais, J.M. McDonald, V. Scherr, and S.P. McGlynn, Chemical Reviews 71, 73 (1971).

15. J.G. Calvert and J. Pitts, Photochemistry (John Wiley and Sons, Inc, New York, 1966).

16. C.K. Luk and R. Bersohn, J. Chem. Phys. 58, 2153 (1973). The authors analyze the build-up time of the fluorescence to determine $\tau_{ICN} \leqslant 5\times10^{-10}$ sec.

17. H.E. Radford and H.P. Broida, Phys. Rev. 128, 231 (1962).

18. W.M. Jackson, J. Chem. Phys. 61, 4177 (1974).

19. R.G. Bennett and F.W. Dalby, J. Chem. Phys. 36, 399 (1962).

20. H.S. Liszt and J.E. Hesser, Astrophys. J. 159, 1101 (1970).

21. K.A. Mohamed, G.C. King, and F.H. Read, J. Elec. Spec. & Rel. Phen. 12, 229 (1977).

22. J.H. Moore and D.W. Robinson, J. Chem. Phys. 48, 4870 (1968).

23. A. Mele and H. Okabe, J. Chem. Phys. 51, 4798 (1969).

24. W.M. Jackson and J.L. Faris, J. Chem. Phys. 56, 95 (1972).

25. A similar kinetic analysis can be found in: M. Stock, E.W. Smith, R.E. Drullinger, and M.M. Hessel, J. Chem. Phys. 68, 4167 (1978).

26. H.C. Brashears, Jr. and D.W. Setser, Appl. Phys. Lett. 33, 821 (1978).

27. J.G. Eden and R.W. Waynant, Opt. Lett. 2, 13 (1978).

28. C.H. Fisher and R.E. Center, J. Chem. Phys. 69, 2011 (1978).

29. J.G. Eden and S.K. Searles, Appl. Phys. Lett. 30, 287 (1977).

30. R. Burnham and N.W. Harris, J. Chem. Phys. 66, 2742 (1977).

31. R. Burnham and S.K. Searles, Paper AA-3, 30th Annual Gaseous Electronics Conf., Palo Alto, California (1977).

32. J.J. Ewing, 7th Winter Colloquium on Quantum Electronics, Park City, Utah (1977).

Table 1

Results of Linear Least-Squares Fits of τ^{-1} vs P ‡

λ_{ex} (Å)	$\tau^{rad}_{CN(B^2\Sigma^+)}$ (nsec)	k_q^{ICN} (cm^3-s^{-1})
1698	70.1(10)	$1.15(2)\times10^{-9}$
1575	66.9(15)	$9.8(4)\times10^{-10}$
1480	71.8(20)	$1.15(5)\times10^{-9}$
1402	73.3(14)	$1.31(3)\times10^{-0}$
*	70.5(16)	$1.15(4)\times10^{-9}$

*Data from all four wavelengths used in a single fit of τ^{-1} vs P.

‡ Stern-Volmer plots, see Figs. 4 and 5. $\tau_{CN^*(B^2\Sigma^+)}$ denotes the inverse of the intercept of the τ^{-1} vs P plots and k_q^{ICN} represents the slope. e.s.d.'s are in parentheses.

Table 2

Ratio of Integrated Intensities of Decay Components Obtained With ICN Sample

λ_{ex} (Å)	$I^{tot}_{short}/I^{tot}_{CN(B^2\Sigma^+)} \times 10^2$
1698	28
1575	3
1480	7
1402	9

Table 3

Summary of $CN^*(B^2\Sigma^+)$ Lifetime Measurements

$\tau_{CN^*(B^2\Sigma^+)}$ (nsec)	Method	Remarks	Ref.
65.6(10)	Pulsed laser-induced fluorescence[a]	v' = 0	18
60.8(20)	Pulsed VUV photolysis (broadband) of ICN and BrCN[a]	Several vibrational states of CN* probed	16
85(6)	Pulsed electron-bombardment[a]	Several vibrational states of CN probed	19
59.3(60)	Phase-shift technique with electron bombardment excitation	v' = 0,1,2	20
61.1(76)	Photon-photon delayed coincidence following electron bombardment excitation	v' = 0,1	21
63.8(6)	Pulsed electron bombardment excitation[a]	v' = 0	11
82(9)	Phase-shift using electron impact	v' = 0,1,2,3,4	22
70.5(20)	See text	Several vibrational states of CN probed	Present work

[a]Fluorescence decay directly observed.

Table 4

Compilation of XeF* Lifetime Results

$\tau_{XeF^*B^2\Sigma^+}$(nsec)	$\tau_{XeF^*C^2\Pi_{3/2}}$(nsec)	Method	Remarks	Ref.
14.25(20)		XeF_2 photolysis at 1750 Å		27
19.4(10)		Laser-induced fluorescence	a	28
16.5(50)		Pulsed electron bombardment excitation of XeF_2		29
18.8		XeF_2 photolysis at 1930 Å	a	30
15.0(8)				31
13.5(10)	100-150			32
12	113	Calculation (Hartree-Fock with CI, semi-empirical inclusion of spin-orbit effects		2
14.2(2)	98(10)	See text		Present work

[a]At time of these references, the $A^2\Pi_{3/2,1/2}$ were denoted as two states and the $B^2\Sigma^+_{1/2}$ was denoted as the C state.

Figure Captions

Figure 1. Experimental schematic.

Figure 2. ICN excitation spectrum (fluorescence intensity vs excitation wavelength; uncorrected for variations in incident radiation flux).

Figure 3. ICN decay curve ($CN^*(B^2\Sigma^+)$ decay only).

Figure 4. Individual ICN Stern-Volmer fits.

Figure 5. Stern-Volmer fit (all four wavelengths).

Figure 6. Unfiltered decay curve with ICN as sample gas.

Figure 7. XeF* decay curve.

Figure 8. XeF* Stern-Volmer fits.

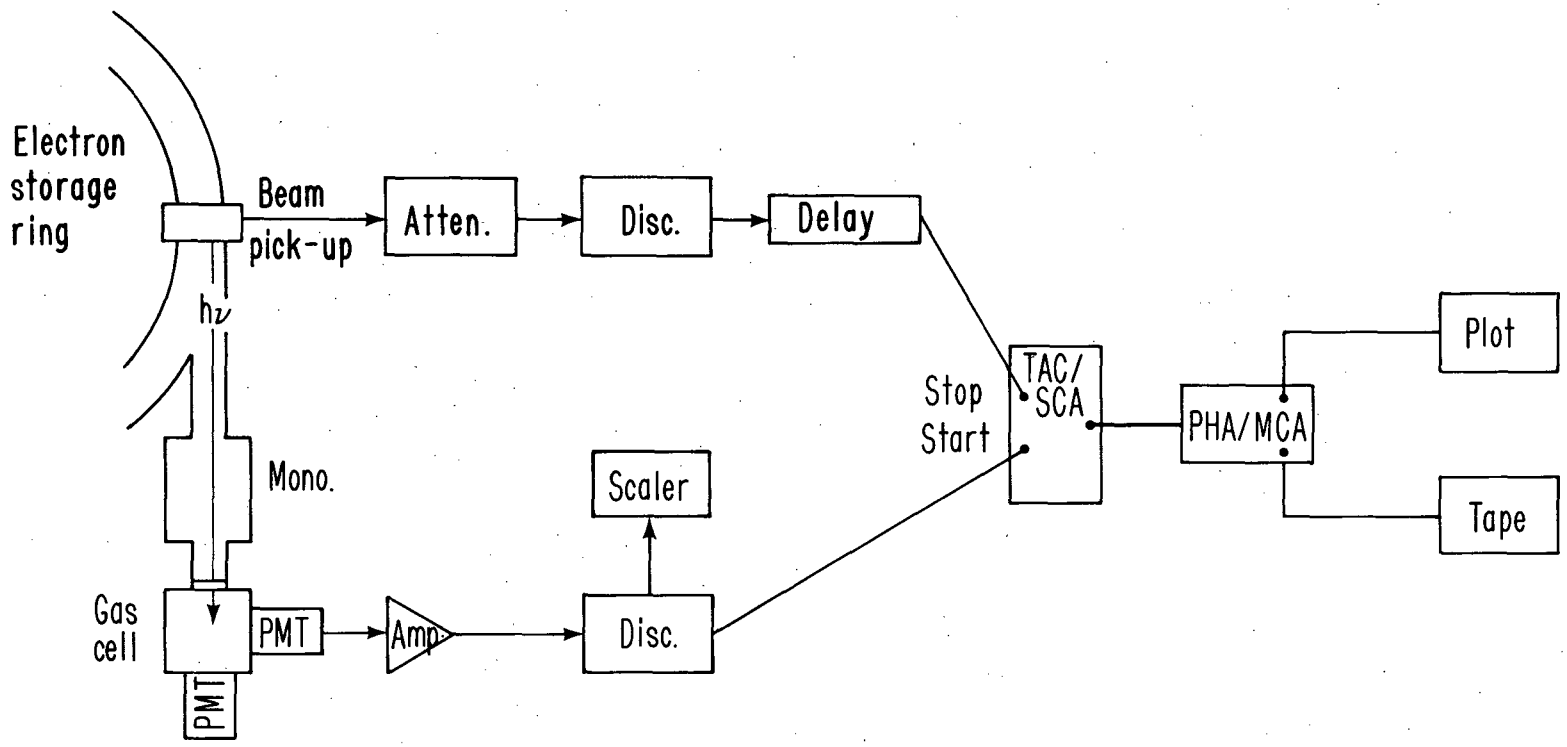

XBL-7612-4530

Figure 1

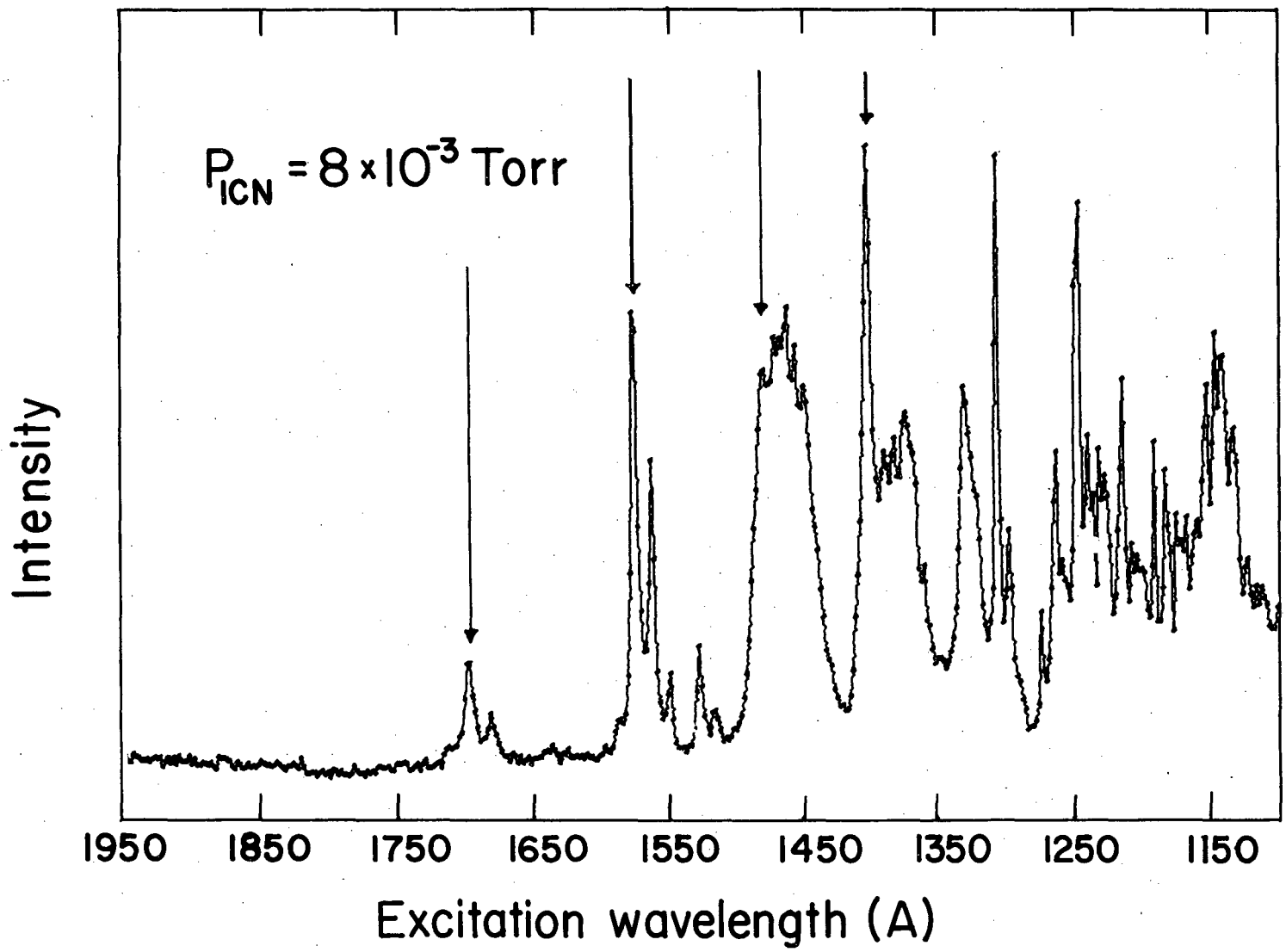

XBL 7810-11909

Figure 2

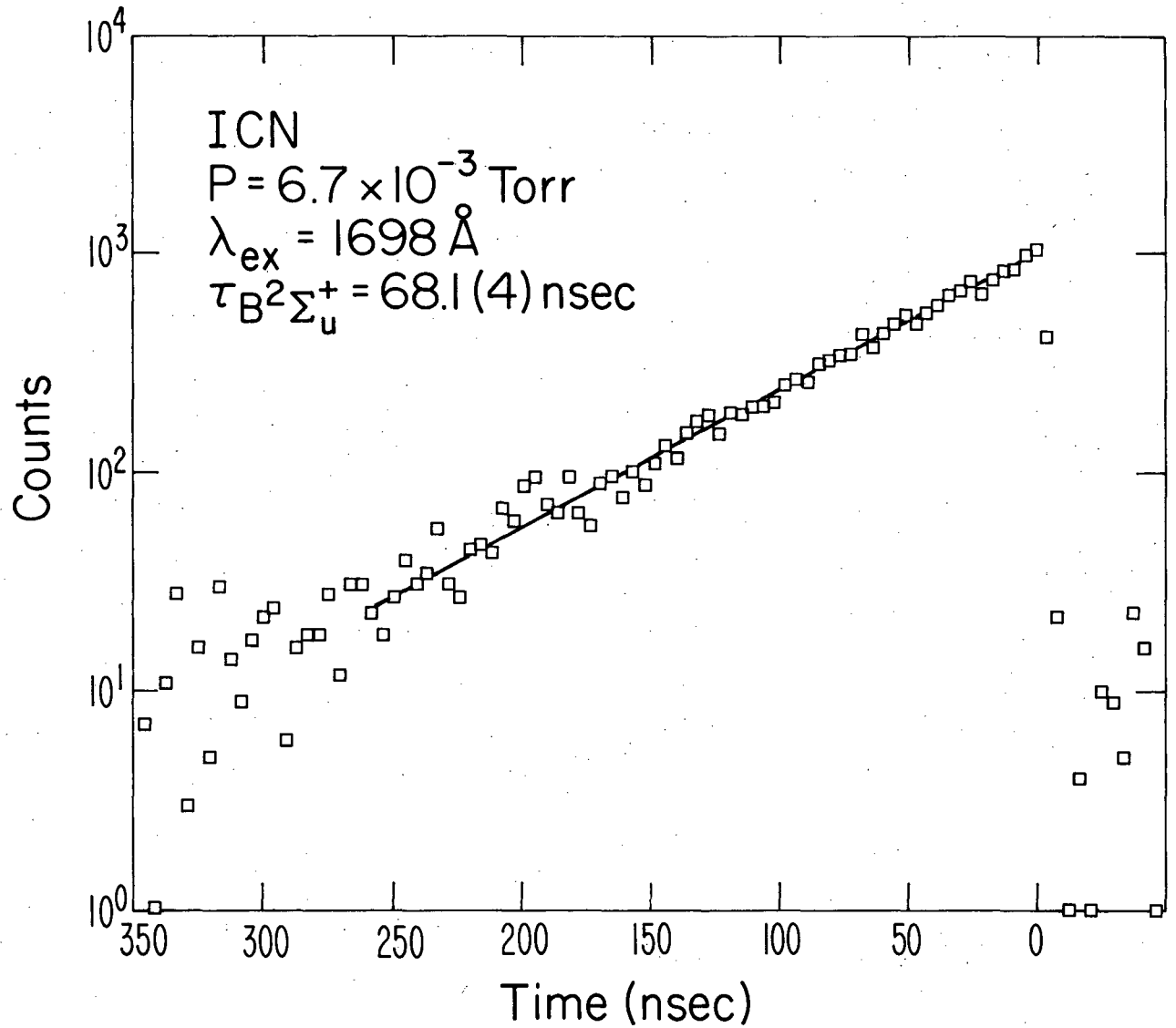

XBL797-2094

Figure 3

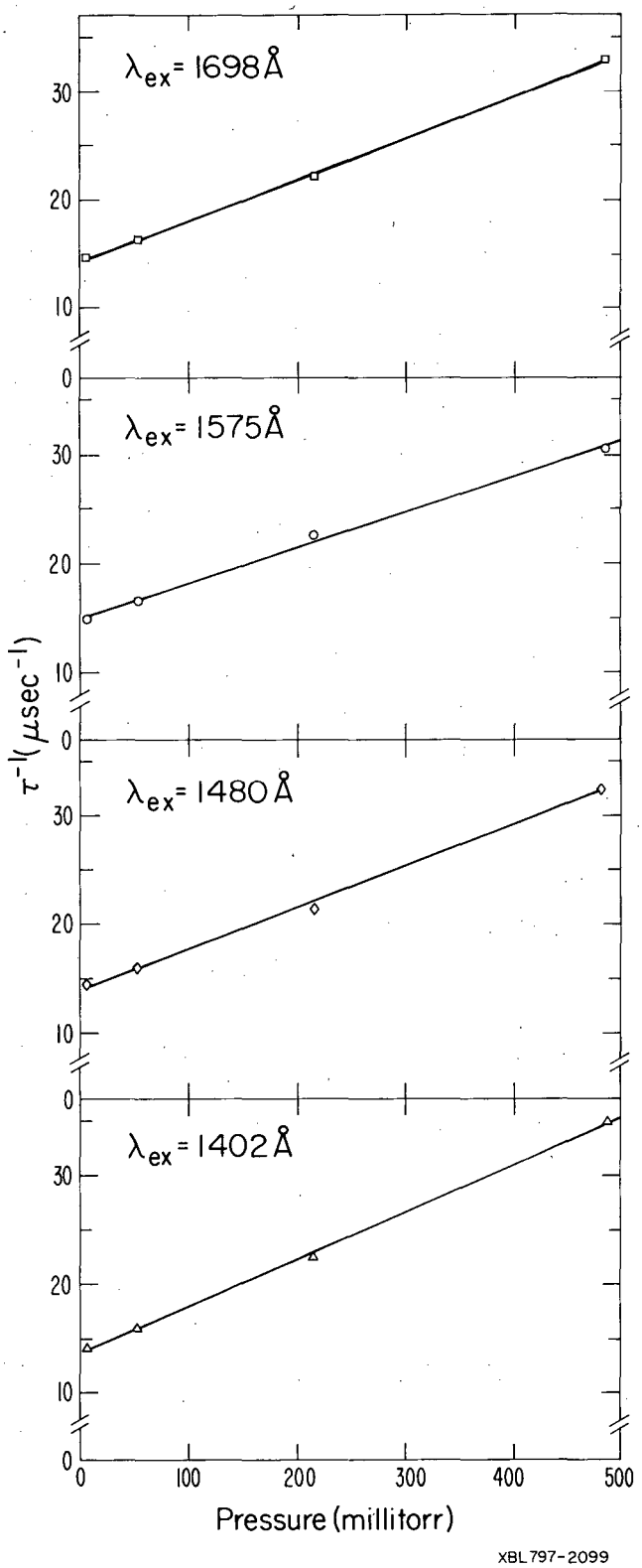
λex = 1698 Å
λex = 1575 Å
λex = 1480 Å
λex = 1402 Å
τ⁻¹ (μsec⁻¹)
0
10
20
30
0
100
200
300
400
500
Pressure (millitorr)
XBL 797-2099

Figure 4

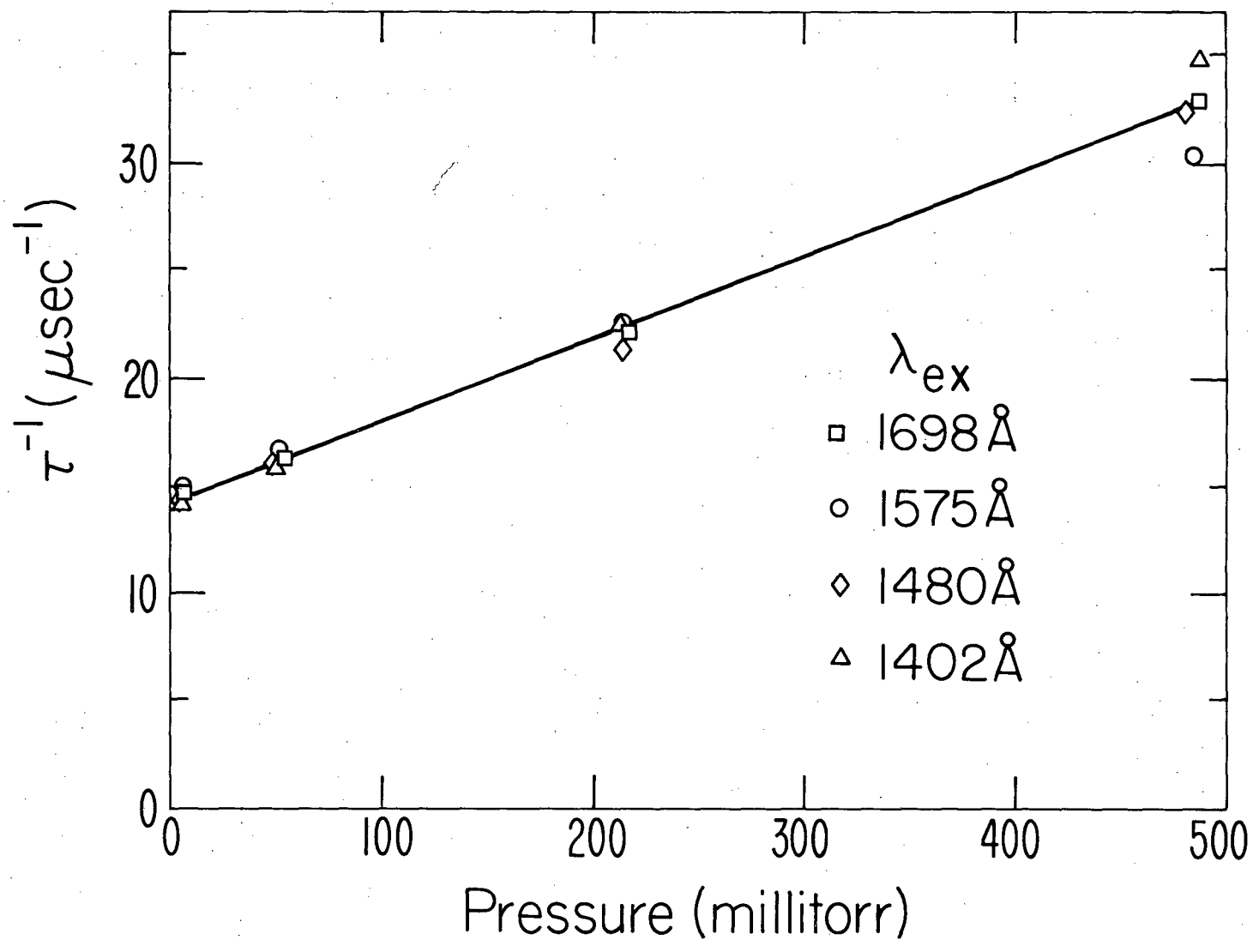

XBL797-2098

Figure 5

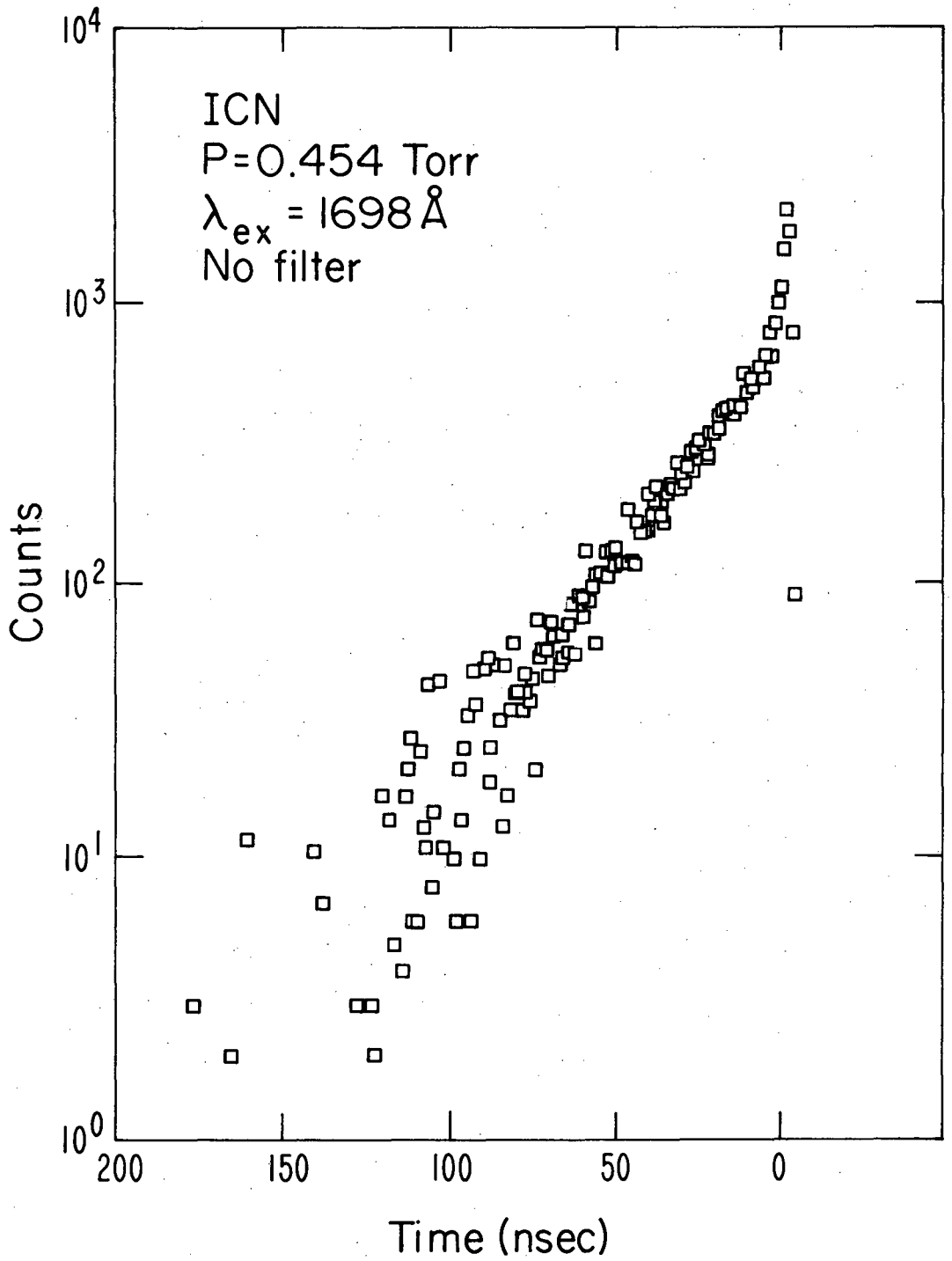

XBL797-2095

Figure 6

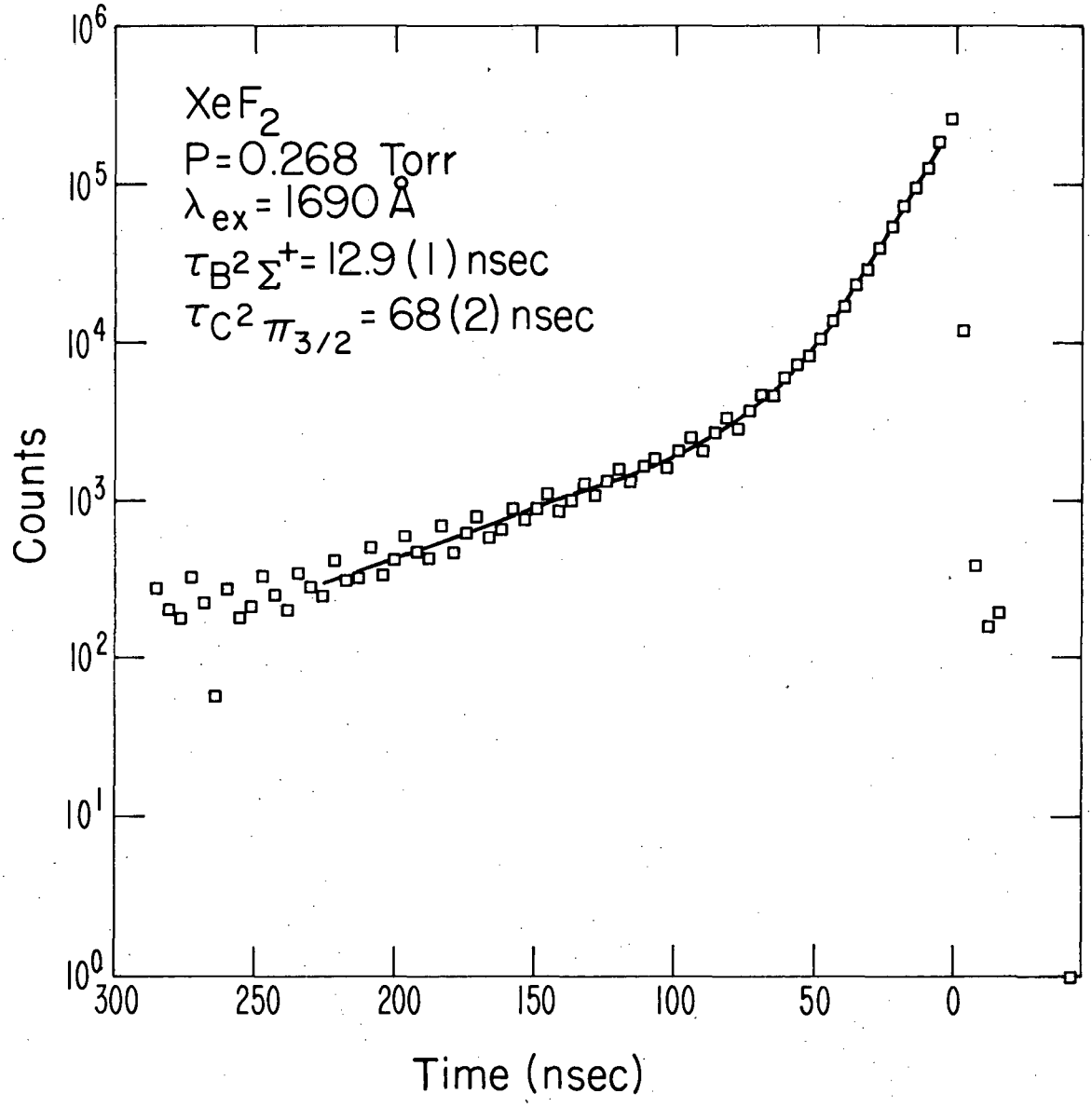

XBL 797-2096

Figure 7

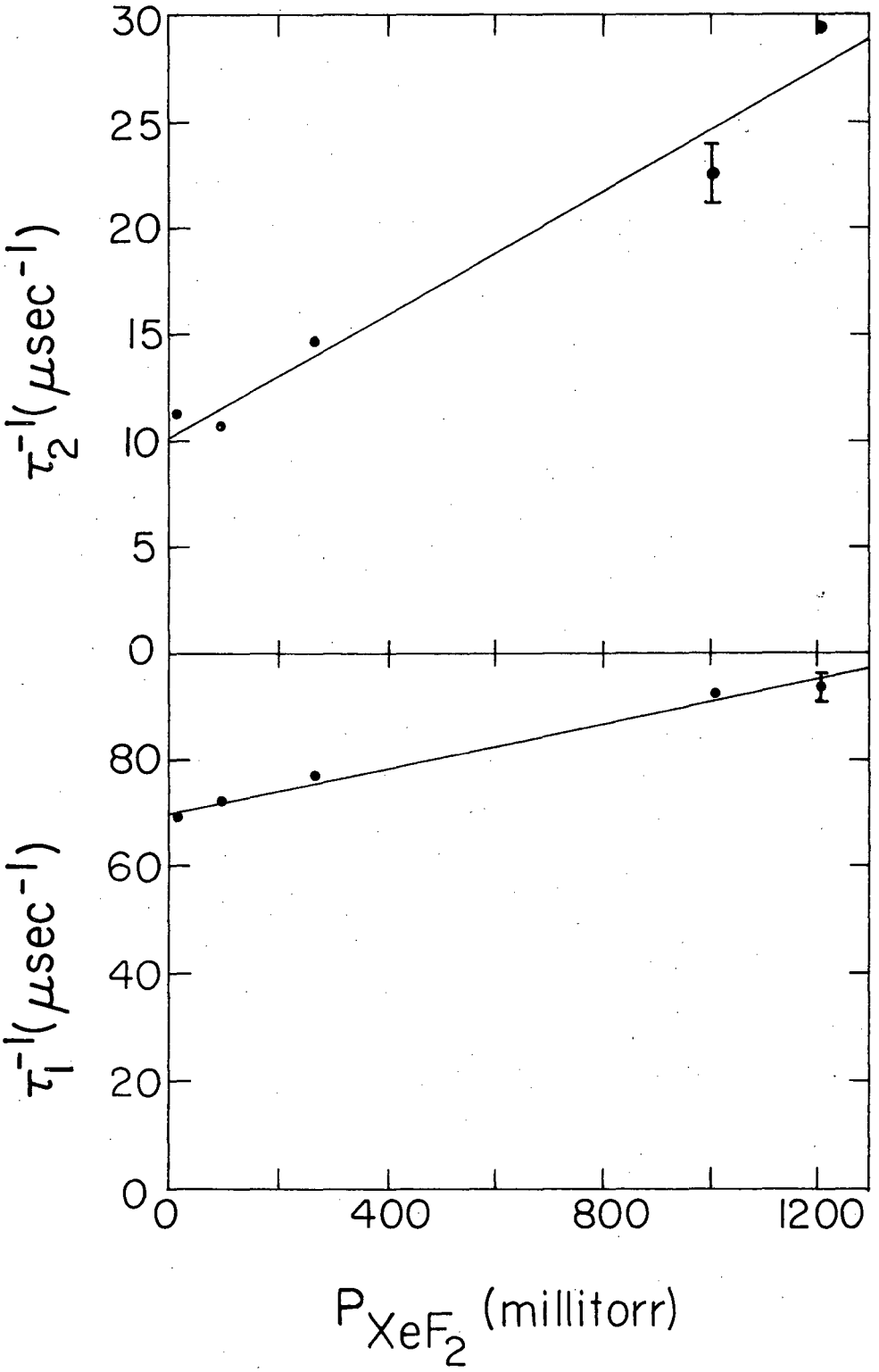

XBL 797-10657

Figure 8

This report was done with support from the Department of Energy. Any conclusions or opinions expressed in this report represent solely those of the author(s) and not necessarily those of The Regents of the University of California, the Lawrence Berkeley Laboratory or the Department of Energy.

Reference to a company or product name does not imply approval or recommendation of the product by the University of California or the U.S. Department of Energy to the exclusion of others that may be suitable.

TECHNICAL INFORMATION DEPARTMENT
LAWRENCE BERKELEY LABORATORY
UNIVERSITY OF CALIFORNIA
BERKELEY, CALIFORNIA 94720